

PAPER

The alternating-sign magnetoresistance of polycrystalline manganese chalcogenide films

To cite this article: S S Aplesnin *et al* 2018 *Semicond. Sci. Technol.* **33** 085006

View the [article online](#) for updates and enhancements.

Related content

- [Ferromagnetic and antiferromagnetic semiconductors](#)
E L Nagaev
- [Low field magnetotransport in manganites](#)
P K Siwach, H K Singh and O N Srivastava
- [Lanthanum manganites and other giant-magnetoresistance magnetic conductors](#)
E L Nagaev

Recent citations

- [Low-temperature phase transition in bismuth ferrite films substituted by manganese](#)
S S Aplesnin *et al*



IOP | ebooks™

Bringing together innovative digital publishing with leading authors from the global scientific community.

Start exploring the collection—download the first chapter of every title for free.

The alternating-sign magnetoresistance of polycrystalline manganese chalcogenide films

S S Aplesnin^{1,2}, O B Romanova¹ , M N Sitnikov², V V Kretinin²,
A I Galyas³ and K I Yanushkevich³

¹Kirensky Institute of Physics, Federal Research Center KSC SB RAS, Akademgorodok 50, bld. 38, 660036 Krasnoyarsk, Russia

²Reshetnev Siberian State University of Science and Technology, Krasnoyarskii rabochi Ave. 31, 660014 Krasnoyarsk, Russia

³Scientific-Practical Materials Research Center NAS of Belarus, P. Brovki Str. 19, 220072 Minsk, Belarus

E-mail: rob@iph.krasn.ru

Received 12 March 2018, revised 21 May 2018

Accepted for publication 21 June 2018

Published 11 July 2018



CrossMark

Abstract

The correlation between the dc and ac electrical resistance and the structural, magnetic, and thermoelectric properties of polycrystalline $\text{MnSe}_{1-x}\text{Te}_x$ ($0.3 \leq x \leq 0.4$) manganese chalcogenide films in the temperature range of 80–400 K has been investigated. Inhomogeneous electronic states and transitions between them accompanied by structural lattice deformations have been found at temperatures including the Neel temperature region. The magnetic susceptibility maximum above the Neel temperature in a magnetic field of 8.6 kOe has been observed. Temperature ranges of the coexistence of two types of electrically inhomogeneous states have been established by impedance spectroscopy in the frequency range of 0.1–1000 kHz and the change of the hopping conductivity for diffusion one accompanied by the magnetic susceptibility minimum has been found. The magnetoresistance in magnetic fields of up to 12 kOe has been established. It has been revealed that the thermopower and magnetoresistance change its sign upon heating. The experimental data are explained using a spin polaron model with the localization of polarons and formation of the electron phase-separation. The alternation of magnetoresistance in sign is attributed to the ferromagnetic orbital ordering of electrons and the negative magnetoresistance is explained by suppression of spin fluctuations in a magnetic field.

Keywords: polycrystalline films, magnetoresistance, impedance, polaron, magnetic properties, thermoelectric

1. Introduction

In recent years, the 3d-metal chalcogenides have been objects of intense study. The interest in these compounds has increased after the discovery of superconductivity in $\text{FeSe}_{1-x}\text{Te}_x$ iron chalcogenides [1]. The superconductivity of these materials was assumed to be implemented via the electron–phonon interaction and magnetic and electron–electron correlations [2]. The orbital-selective Cooper pairing based mainly on d_{xz} electrons of iron atom orbitals in FeSe was found [3]. The role of magnetic order in controlling the transport characteristics in $\text{FeSe}_{1-x}\text{Te}_x$ was investigated [4]. The anion substitution enhances the interplay of the electron, magnetic, and elastic subsystems of a compound. Substitution

of manganese for iron retains these properties. Manganese monoselenide and monotelluride are p-type semiconductors, which undergo the structural and magnetic transitions with an increase in the degree of hybridization of manganese cations with Se and Te anions. The initial MnSe compound has the polymorphic properties, which consist in the coexistence of different crystal structures [5]. At temperatures of $248 \text{ K} < T < 266 \text{ K}$, manganese monoselenide undergoes the structural phase transition from the cubic phase to the NiAs structure; below these temperatures, two phases coexist in a sample. The temperature of the magnetic phase transition in MnSe in its cubic modification is $T_N = 135 \text{ K}$; in the NiAs hexagonal phase, it coincides with the temperature $T_s = 272 \text{ K}$ of the structural transition [6].

Manganese monotelluride in the α modification has a NiAs-type hexagonal structure [7]; it is an antiferromagnet with a Neel temperature of $T_N = 310$ K [8]. The transport and magnetic measurements of manganese monotelluride revealed several low-temperature anomalies, including the negative electrical resistance coefficient below 100 K and the sharp susceptibility growth at $T \sim 83$ K [9]. The bulk MnTe sample exhibits the unique properties under pressure, since in this case its Neel temperature increases, attaining $T_N = 520$ K at $P = 8$ GPa, and the gap in the electron excitation spectrum halves and correlates with a decrease in the metal-anion bond length R_A . According to the theoretical calculation, the hexagonal (H) crystal structure changes for the cubic (ZB) structure with the antiferromagnetic ordering with an energy difference of $\Delta E_{ZB,H} = -0.21$ eV/bond per one Mn-Te bond with a length of $R_{AF} = 0.27$ nm and with the ferromagnetically ordered spins with an energy difference of $\Delta E_{ZB,H} = -0.40$ eV/bond per bond with a length of $R_F = 0.271$ nm (compare with the binding energy in the NiAs structure with R (Mn-Te) = 0.273 nm [10]). The results of theoretical calculations agree well with the experimental data obtained on MnTe thin films. The thin-film compounds formed on a substrate with the cubic symmetry in the [100] direction are ferromagnets with the cubic structure, which have the minimum electrical resistance in the vicinity of the Curie temperature. The films on the substrate in the [111] direction are antiferromagnets with the maximum electrical resistance in the vicinity of the Neel temperature. In the MnSe and MnTe chalcogenides, the Neel temperature and activation energy decrease at the transition from bulk samples to thin-film compounds. In the MnSe compounds, the cubic structure stabilizes [11]. The galvanomagnetic properties, Neel temperature, and resistivity depend on film thickness and substrate temperature [12, 13].

In the bulk $\text{MnSe}_{1-x}\text{Te}_x$ samples [6], substitution of tellurium for selenium retains the cubic and magnetic structure. In the $\text{MnSe}_{1-x}\text{Te}_x$ compound with $X = 0.1$ [14, 15], the 100% negative magnetoresistance near the Curie temperature was established. The magnetoresistive effect weakens with increasing tellurium concentration and vanishes at $X = 0.3$. The negative magnetoresistive effect in the bulk MnSe samples is 14% in the magnetically ordered cubic phase [16]; in MnTe, the effect is not observed. However, the thin-film MnTe samples exhibit the magnetoresistance with a maximum at 200 K [17].

The positive magnetoresistance was found in topological insulators [18]. In the bulk Bi_2Te_3 sample, the room-temperature magnetoresistance is about 15%, while in Bi_2Te_3 thin films the giant magnetoresistive effect attains 600% at room-temperature [19, 20]. The observed high room-temperature magnetoresistance values are directly related to a decrease in the dimensionality of a topological insulator. The magnetoresistance of the Bi_2Se_3 films with a thickness of 200 nm linearly depends on temperature and remains in strong magnetic fields and in the high-temperature range [21]. The magnetoresistive effect is explained by the presence of high carrier mobility channel, which coexists in the Bi_2Se_3 thin

films with a conventional bulk channel with a mobility of $16 \text{ cm}^2 \text{ V}^{-1} \text{ S}^{-1}$ at high temperatures [22]. As the temperature decreases, the carrier density in the high-mobility channel significantly decreases and free carriers are frozen below 85 K; only the bulk conductive channel remains in the film.

The positive magnetoresistance can originate from the competition of the degenerate orbital states of an electron and strong electron correlations [23]. Near the temperature of the transition from the orbitally ordered phase to the paraphrase, the spectral weight of the electron density of states shifts to the Fermi level. In this temperature range, the gap width and orbital ordering temperature increase in a magnetic field. In narrow-gap semiconductors ($W = 1$ eV), the temperature of the magnetoresistive effect attains $T \approx 600$ K [23].

The resistance growth in the antiferromagnetic Sr_2CrWO_6 thin films in a magnetic field is attributed to the suppression of the long-range antiferromagnetic order and formation of a fluctuation region with the short-range order, which enhances electron scattering [24].

The aim of this study was to clarify the magnetoresistance mechanism by complex investigations of the structural, magnetic, and kinetic properties of the polycrystalline nanostructured anion-substituted Mn-Se-Te films in a magnetic field.

2. Synthesis, structure, and magnetic properties of the films

The polycrystalline $\text{MnSe}_{1-x}\text{Te}_x$ ($0.3 \leq X \leq 0.4$) thin-film manganese chalcogenide compounds were synthesized by deposition of previously obtained solid solutions onto object glasses by a flash technique. The precursors used were powders with a gran size from 0.1 to 0.3 mm. Deposition was performed on a UVN-71R-2 vacuum facility. The pressure in a reaction chamber during deposition was 10^{-2} – 10^{-3} Pa. The tantalum evaporator temperature was ~ 2000 °C. Substrates were mounted at a distance of 10 cm from the evaporator. The substrate temperature during deposition was 250 °C–300 °C.

The evaporator temperature was much higher than the solid solution melting point. Therefore, a small amount of the substance hitting the evaporator immediately evaporated, which ensured the formation of structure and composition corresponding to those of bulk substances after crystallization on a substrate significantly distant from the evaporator. The precursor was supplied to the evaporator with a shock vibration device. The film thickness varied from 157 to 960 nm. The substrate material was quartz.

X-ray diffractometry (XRD) investigations of the $\text{MnSe}_{1-x}\text{Te}_x$ ($0.3 \leq X \leq 0.4$) thin-film chalcogenide compounds were carried out on a DRON-3 diffractometer (CuK α radiation) at a temperature of 300 K after fabrication of the samples and after the measurements of their magnetic and electrical properties. The structure of thin-film compounds differs from the face-centered cubic (fcc) structure of bulk

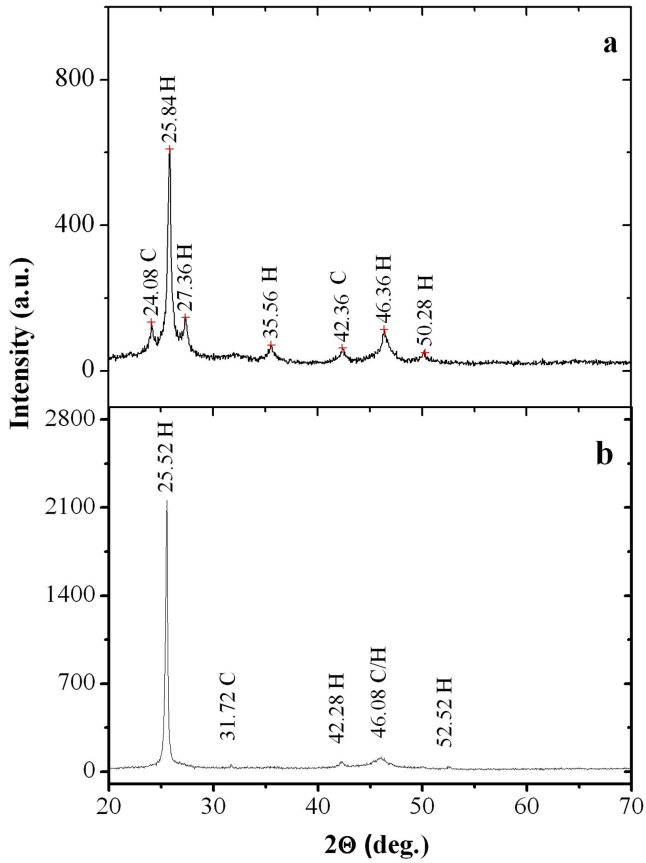


Figure 1. XRD patterns of the thin-films $\text{MnSe}_{0.7}\text{Te}_{0.3}$ (a) and $\text{MnSe}_{0.6}\text{Te}_{0.4}$ (b) H-hexagonal; C-cubic phase.

Table 1. Structural characteristic of thin-film system $\text{MnSe}_{1-x}\text{Te}_x$ samples.

Compositions	a , nm	c , nm	c/a
$\text{MnSe}_{0.7}\text{Te}_{0.3}$	0.393 32	0.554 44	1.4
$\text{MnSe}_{0.6}\text{Te}_{0.4}$	0.395 85	0.563 13	1.42

polycrystalline $\text{MnSe}_{1-x}\text{Te}_x$ samples with the same Te concentration [17]. According to the XRD data, substitution of tellurium for selenium in the $\text{MnSe}_{1-x}\text{Te}_x$ thin-film chalcogenides leads to a decrease in the cubic structure peak intensities and causes the occurrence of the nickel arsenide (NiAs) hexagonal structure (figure 1). The ratio of these phases in the films depends on concentration. For $X = 0.3$, the weight of the cubic phase with respect to the hexagonal phase is 28%, and for $X = 0.4$ this ratio decreases to 5%. The lattice parameter increases with the tellurium concentration. The unit cell volume in the NiAs-type hexagonal structure decreases as compared with the bulk MnTe sample and the c/a ratio in the film is smaller than its value of 1.63 in the bulk sample [25] (table 1).

The magnetic moments of the films were measured by a ponderomotive technique in a magnetic field of 8.6 kOe in the temperature range of 80–1000 K on the samples placed into evacuated quartz ampules. Figures 2(a) and (b) show

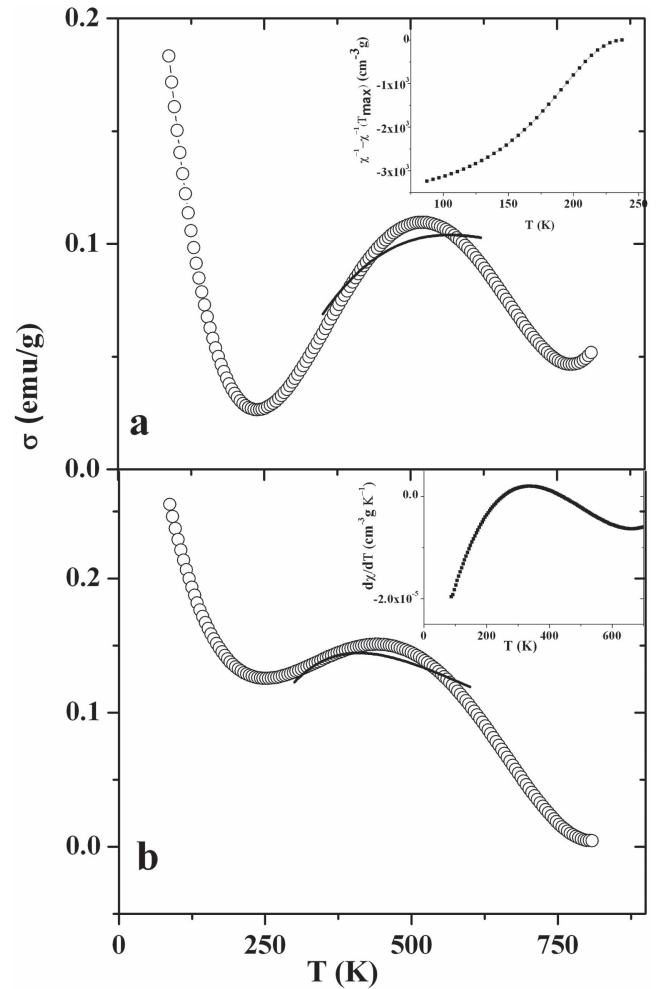


Figure 2. The temperature dependence of the magnetization of the films $\text{MnSe}_{0.7}\text{Te}_{0.3}$ (a) and $\text{MnSe}_{0.6}\text{Te}_{0.4}$ (b) measured in a magnetic field of 8.6 kOe. Solid lines represent fitting parameters by function $M = A \exp(-3E_0/2kT)/T^3$. Insert: (a) the temperature dependence of normalized function of the susceptibility for $\text{MnSe}_{0.7}\text{Te}_{0.3}$; (b) the derivative of the susceptibility for $\text{MnSe}_{0.6}\text{Te}_{0.4}$.

temperature dependences of magnetization of the $\text{MnSe}_{1-x}\text{Te}_x$ ($X = 0.3$ and 0.4) thin-film chalcogenide compounds. The dependences are qualitatively different from the $\sigma(T)$ curves for bulk $\text{MnSe}_{1-x}\text{Te}_x$ samples [26]. The films exhibit the maximum magnetization at 500 K, which is related to the formation of spin polarons above the Neel temperature.

The increase in magnetization with lowering temperature is associated with the magnetic orbital moments of manganese electrons in the cubic phase and is not determined by the paramagnetic contribution. According to the phase relationship, this contribution decreases with increasing concentration and a significant decrease in the magnetization growth is observed. The temperatures of magnetic transition in the $\text{MnSe}_{1-x}\text{Te}_x$ compound (340 and 320 K for substitute concentrations of $X = 0.3$ and 0.4) was determined from the maximum temperature derivative of susceptibility (insert to figure 2(b)). The theoretical calculations of the NiAs electronic structure in MnTe yielded the magnetic moment range of 4.17–4.3 μ_B on manganese ions and 0.05–0.14 μ_B on tellurium anions [9]. The electron densities on manganese and

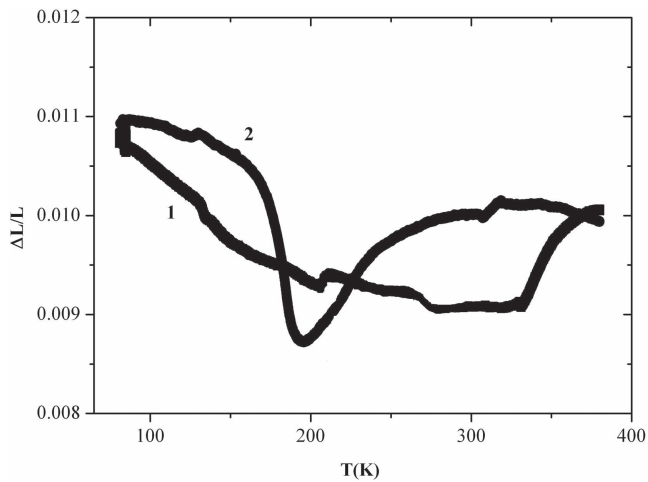


Figure 3. The temperature dependence of the relative linear size variation $\text{MnSe}_{0.7}\text{Te}_{0.3}$ (a) and $\text{MnSe}_{0.6}\text{Te}_{0.4}$ (b) films.

tellurium ions are different from five and two electrons and the effective valences of ions are $\text{Mn}^{+2+\delta}$ and $\text{Te}^{-2-\delta}$. Manganese ions in the NiAs hexagonal structure form an octahedron and a hole on the e_g orbital upon hybridization will lead to the double exchange. In bulk manganese tellurides, the antiferromagnetic exchange along the hexagonal axis exceeds the ferromagnetic exchange in the plane by an order of magnitude. Above the Neel temperature, the spin polaron is vanished at the temperature corresponding to the maximum magnetic susceptibility.

The lattice strain under the electron-lattice and magnetoelastic interactions can be determined from the relative linear size variation $\Delta L/L$ in the $\text{MnSe}_{1-x}\text{Te}_x$ films with $X = 0.3$ and 0.4 . We measured the electrical resistance of strain gauges placed in the sample and quartz $(R^s(T) - R^q(T))/R^q(T) = (L^s(T) - L^q(T))/L^q(T) = \Delta L$. The linear expansion coefficient of quartz is $0.8 \times 10^{-6} \text{ 1/K}$. Figure 3 shows the relative film length variation as a function of temperature. For bulk samples of the $\text{MnSe}_{1-x}\text{Te}_x$ system, the curve $\Delta L/L(T)$ increases monotonically with increasing temperature. In thin MnTe films with NiAs structure, the temperature coefficient of resistance $1/R\Delta R/\Delta T$ has a maximum at 210 K [17] which cause to the localization of polarons and deformation of the lattice. In films with $X = 0.4$, the deformation is due to the pinning of the polarons, and in the film with $X = 0.3$ the deformation is caused mainly by a polymorphic transition from the cubic phase to the hexagonal phase. In the bulk $\text{MnSe}_{0.5}\text{Te}_{0.5}$ samples, the NiAs structure lattice parameters increase by 0.5% below $T = 200$ K, which is consistent with our data. In the region of the transition to the magnetically ordered state ($300 < T < 340$ K), the hexagonal phase exhibits a kink in the temperature dependence of $\Delta L/L$, which is caused by the magnetoelastic interaction.

The magnetization minimum $\sigma(T)$ is not related to the structural transition, but is most likely caused by a change in the electronic structure. The anomalous behavior of the structural and magnetic characteristics in this temperature range reflects on the transport properties.

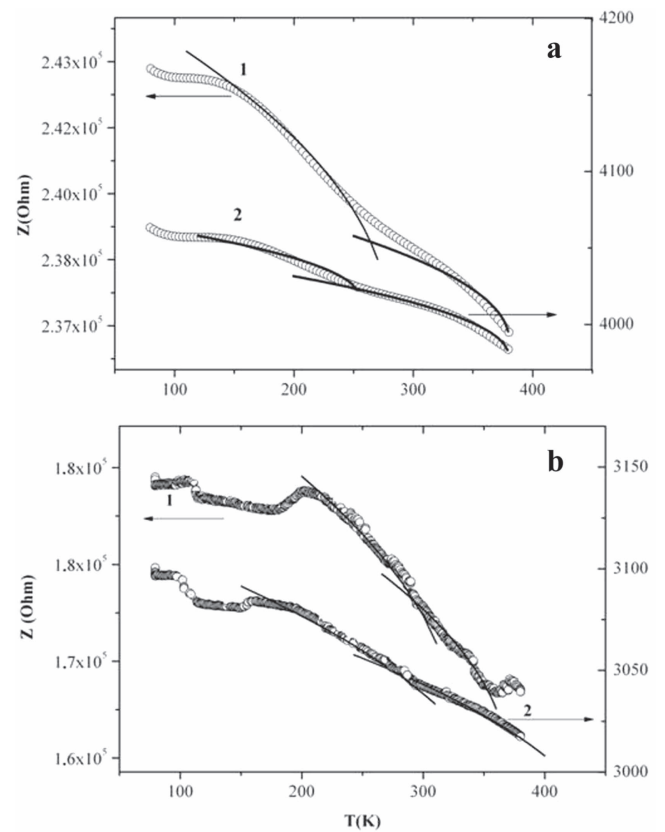


Figure 4. The temperature dependence of the impedance of films $\text{MnSe}_{0.7}\text{Te}_{0.3}$ (a) and $\text{MnSe}_{0.6}\text{Te}_{0.4}$ (b) measured at frequencies of 5 kHz (1) and 300 kHz (2). Solid lines defined fitting functions show two areas one being related to the transition to the magnetically ordered state ($T \geq 240$ K) and the other, to localization of spin polarons in the lattice ($T \leq 240$ K).

3. Results of electrical resistance, impedance, and thermopower

The electrically inhomogeneous states formed by spin and lattice polarons were established by impedance spectroscopy. We measured the active (real part Z') and reactive (imaginary part Z'') of the resistance using an AM-3028 component analyzer and determined full impedance $Z = Z' + iZ''$ of the $\text{MnSe}_{1-x}\text{Te}_x$ ($X = 0.3$ and 0.4) manganese chalcogenide films in the frequency range of $\omega = 1\text{--}1000$ kHz at temperatures of 80–400 K. The temperature dependence of the impedance at both $X = 0.3$ and 0.4 (figures 4(a) and (b)) includes two portions, one being related to the transition to the magnetically ordered state ($200 < T \leq 340$ K) and the other, to localization of spin polarons in the lattice at a temperature of 200 K. According to the linear frequency dependence of the imaginary part of the impedance measured at fixed temperatures, the main contribution to the impedance is made by the capacitance. The imaginary part of the impedance measured at frequencies of 1–1000 kHz is described well by the function $\text{Im} Z = 1/\omega C$ with the capacitance increasing upon heating. The linear $\text{Im} Z(\omega)$ dependence confirms the existence of electrically inhomogeneous states in the film, which are caused by spin polaron pinning.

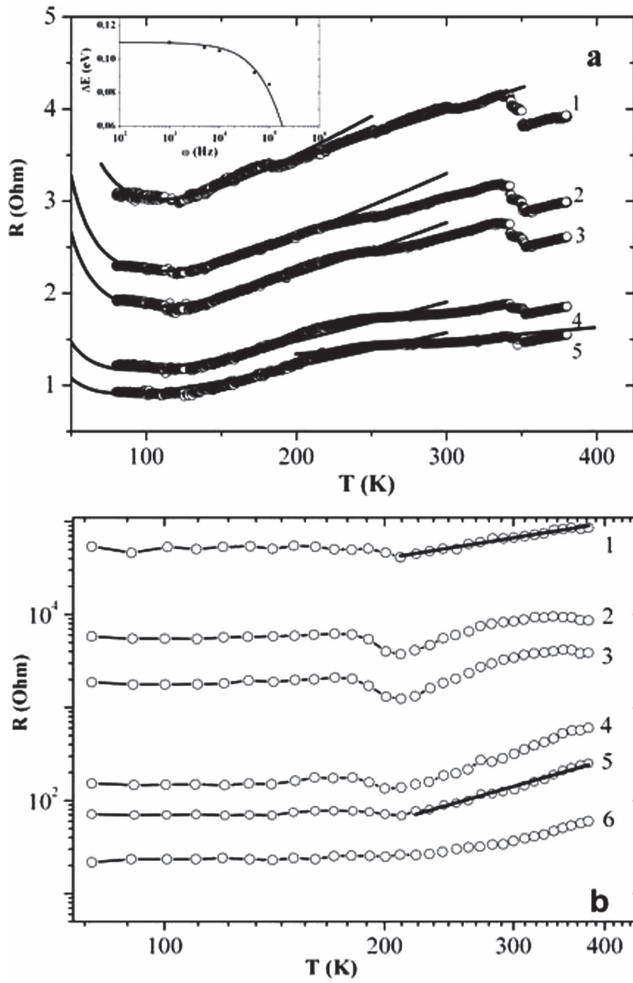


Figure 5. The temperature dependence of the real part of impedance of films $\text{MnSe}_{0.7}\text{Te}_{0.3}$ (a) and $\text{MnSe}_{0.6}\text{Te}_{0.4}$ (b) measured at different frequencies 1 kHz (1), 5 kHz (2), 10 kHz (3), 50 kHz (4), 100 kHz (5) and 300 kHz (6). Inset shows the frequency dependence of the activation energy for the concentration $X = 0.3$. Fitting function (1) is denoted by solid line.

The real part of the impedance monotonically grows upon heating (figures 5(a) and (b)) and decreases with increasing frequency. The ac resistance is caused by scattering of spin polarons on magnons, the density of which increases upon heating. The frequency dependence of the activation energy ΔE determined in the temperature range of 200–340 K in presented in the inset in figure 5(a). It can be seen that the activation energy decreases with increasing frequency according to the power law. The $R(T)$ curves consist of two portions corresponding to the temperature ranges of $80 < T \leq 200$ K and $200 < T \leq 350$ K at both substitute concentrations. A slight kink in the temperature dependence of the resistance is observed for the composition with $X = 0.3$ near the Neel temperature; as the frequency increase, the kink smooths (figure 5(a)). With an increase in the substitute concentration, the real part of the impedance grows by two–four orders of magnitude (figure 5(b)). The singularity in the temperature dependence of $Re(Z)$ at $T \sim 200$ K is consistent with temperature anomalies in the

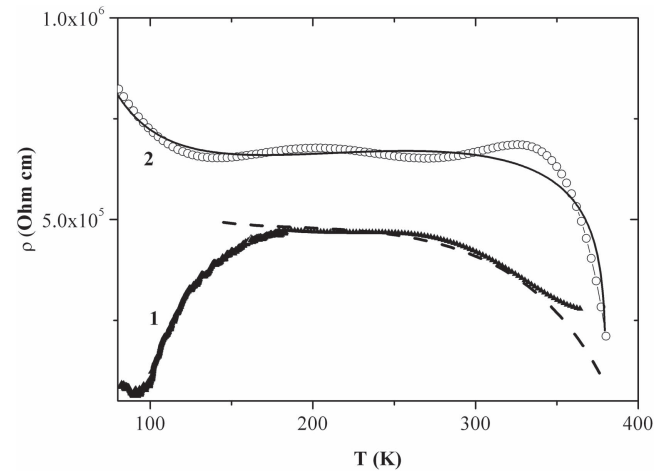


Figure 6. The temperature dependence of the electrical resistivity for films $\text{MnSe}_{0.7}\text{Te}_{0.3}$ (1) and $\text{MnSe}_{0.6}\text{Te}_{0.4}$ (2). The temperature dependence of the resistance is described by the function (2).

structural (figure 3) and magnetic properties (figure 2). Temperature dependences of the impedance and dc resistance are qualitatively different. At low temperatures the resistance increases for film with $X = 0.3$ (figure 6) and the behavior of the $R(T)$ curves in this region for different concentrations has a strong difference. The orbital contribution of electrons give arise to an increase in resistance film with the cubic structure. According to percolation theory, for fcc lattice the percolation concentration is 0.17%, the concentration of the cubic phase exceeds the concentration of percolation and the conductivity is due to a part of the volume of a film with a cubic structure. For a composition with $X = 0.4$, the concentration of the cubic phase is much less than the percolation concentration, and the conductivity is caused by a part of the volume of a film with a hexagonal structure since the of the proportion of cubic phase is much lower than the percolation concentration.

The resistance decreases in the region of the magnetic transition with temperature (figure 6). Localization of spin polarons leads to the lattice strain and a shift in the chemical potential below 200 K. If the chemical potential is located in the quasi-gap formed by the n- and p-type impurity subbands, the electrical resistance grows.

The obtained thermopower data are indicative of the coexistence of two carrier types (figures 7(a) and (b)). Upon heating, the thermopower changes its sign from negative to positive near $T = 164$ K for the composition with $X = 0.3$ and jumps up at $T = 123$ K for the composition with $X = 0.4$, where the thermal expansion coefficient has a local minimum. The temperatures of local thermopower maxima $T(X = 0.3) = 274$ K and $T(X = 0.4) = 260$ K correspond to the temperatures of impedance inflection points dZ/dT and film straining ($T = 269$ K at $X = 0.3$). The thermopower attains its maximum value in the vicinity of the magnetic phase transition temperature. The temperature gradient induces the lattice polaron flux from the high-density to low-density part of the film. The local thermopower maxima are caused by the spin-lattice polaron flux forming upon variation in the charge density wave period.

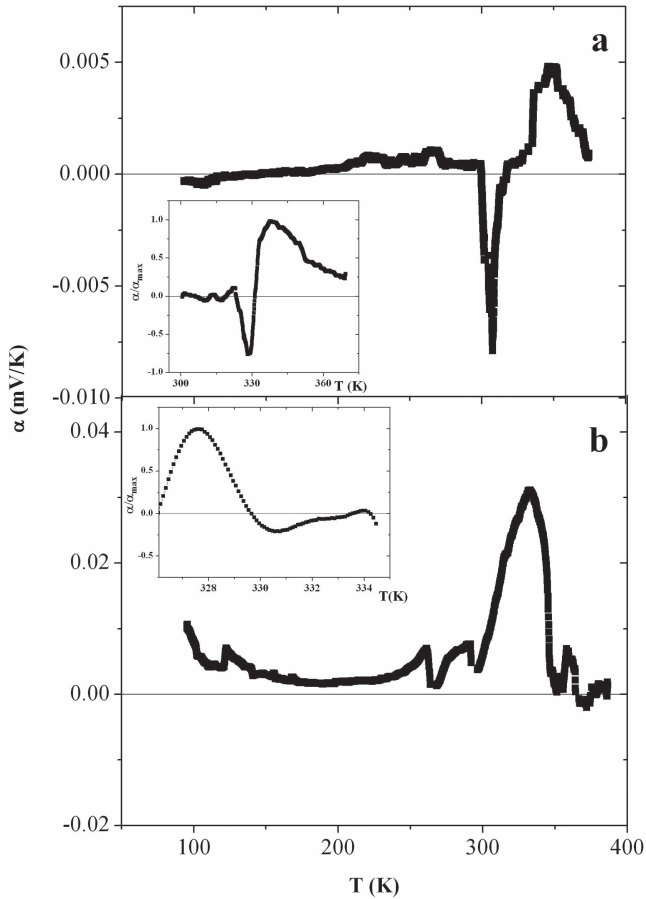


Figure 7. The temperature dependence of the thermopower data for thin-film chalcogenides compounds $\text{MnSe}_{0.7}\text{Te}_{0.3}$ (a) and $\text{MnSe}_{0.6}\text{Te}_{0.4}$ (b). On the inset, the calculated dependences with the parameter $\alpha/\alpha_{\text{max}} = \beta(T)/\beta(T_{\text{max}})$ of the same compositions.

The spin polaron spectrum can be controlled by a magnetic field via the magnetic structure reconstruction. The effect of magnetic field on the transport properties can be determined from the I - V characteristics measured at fixed temperatures without field and in a magnetic field of 12 kOe (figures 8(a) and (b)). The temperature dependences of magnetoresistance $\delta = \rho(H)/\rho(0) - 1$ for the compositions with $X = 0.3$ and 0.4 are presented in figures 9(a) and (b). The magnetoresistance changes its sign upon heating. The positive magnetoresistance is due to the orbital electron contribution and is observed in the low-temperature region. With increasing concentration, the weight of the cubic phase decreases and, accordingly, the orbital contribution of electrons to the magnetoresistance decreases. The maximum decrease $\delta = -23\%$ in the magnetoresistance in a magnetic field is observed at $T = 180$ K for $X = 0.3$ and $\delta = -42\%$ at $T = 160$ K for $X = 0.4$. Above the Neel temperature, the magnetoresistance almost vanishes. The temperature of the maximum negative magnetoresistance is consistent with the temperature of the maximum magnetoresistance in manganese monotelluride films [17]. The electrical resistance monotonically decreases in a magnetic field (see the inset in figure 9(b)).

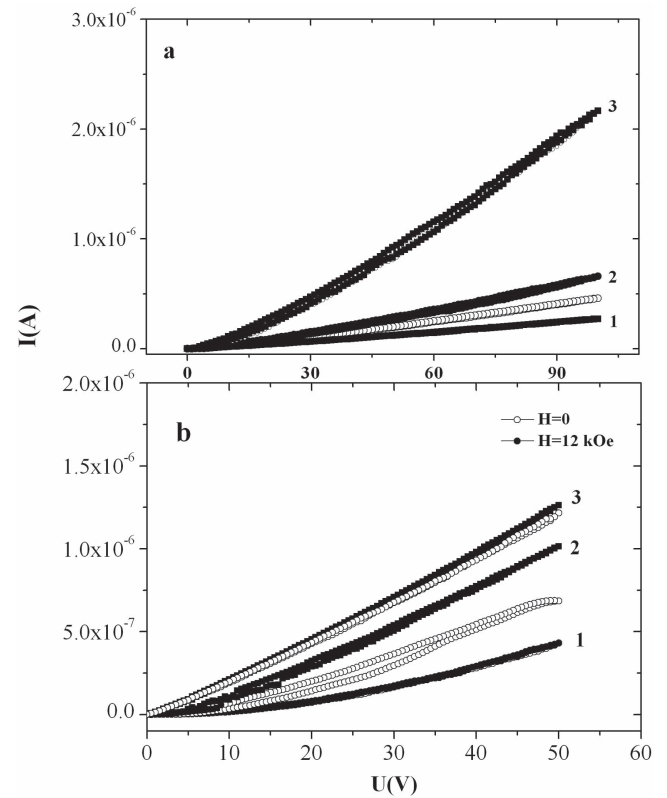


Figure 8. The current–voltage characteristics measured in a zero magnetic field and field 12 kOe. (a) $\text{MnSe}_{0.7}\text{Te}_{0.3}$ at $T = 100$ K (1), 180 K (2) and 240 K (3); (b) $\text{MnSe}_{0.6}\text{Te}_{0.4}$ at $T = 120$ K (1), 160 K (2) and 240 K (3).

4. Model and discussion

Our experimental data can be described using the spin polaron model. The exchange interaction of delocalized electrons with the localized electron spins results in the formation of the ferromagnetic exchange coupling, which competes with the indirect antiferromagnetic exchange. We estimated the size of a ferromagnetic cluster, which can be presented as a sphere with the radius $R = \sqrt{2D\tau}$, where D is the diffusivity of electron in cluster and τ is the spin polaron relaxation time, in the vicinity of the Neel temperature and above it. The cluster magnetic moment is $M \sim (R/a)^3 \mu_B \sim (D\tau)^{3/2} \mu_B$, where a is the lattice constant. Near the Neel temperature, the diffusivity of electron has the activation form $D = A \exp(-E_0/kT)$ caused by absorption of an optical magnon with $E_0 = 0.06$ eV for $X = 0.3$ and $E_0 = 0.05$ eV for $X = 0.4$. The function $M = A \exp(-3E_0/2kT)/T^3$ with the temperature dependence of the relaxation time $\tau \sim 1/T^2$ satisfactory describes the temperature behavior of susceptibility in the temperature range of 350–600 K. Above $T = 500$ –600 K, the optical magnon branch of spin excitations disappears and the correlation radius of the antiferromagnetic ordering decreases, and so does the radius of localization of the electrons inducing the ferromagnetic exchange.

At the transition to the magnetically ordered state, it is energetically more favorable for an electron to form a ferromagnetic region that works as a potential well for it and to

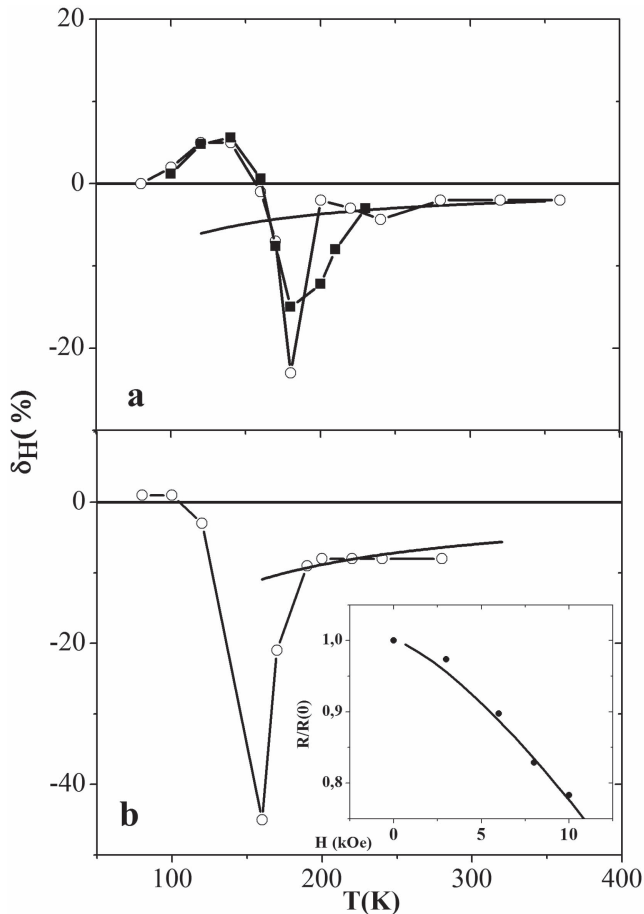


Figure 9. The temperature dependences of the magnetoresistance for $\text{MnSe}_{0.7}\text{Te}_{0.3}$ (a) and $\text{MnSe}_{0.6}\text{Te}_{0.4}$ (b). Inset: field dependence of magnetoresistance at 180 K is described by the function (4) for $\text{MnSe}_{0.6}\text{Te}_{0.4}$. The magnetoresistance is related to the electron hopping mechanism and describes by the functional dependence (3) (solid line) and summation magnetoresistance (dark symbol).

localize in this well. Inside the ferromagnetic region (ferron), the electron energy is shifted downward relative to the antiferromagnetic state by $AS/2$, where A is the constant of exchange coupling between localized and delocalized electrons. The total ferron energy is determined by the potential, kinetic, and exchange coupling (JS) energies [27]. The competition between these interactions determines the ferron radius. Ferrons lead to the modulation of the antiferromagnetic structure with the wave vector $Q \sim 1/R$ [28]. The charged ferron induces the electrical capacitance $C \approx 4\pi\epsilon_0 R$ and the impedance depends on the ferron radius $\text{Im}(Z) = 1/\omega C \sim 1/R \sim Q$. The temperature dependence of the impedance is determined by the charge ordering modulation $Z = Z_0 + Z_1(T)$, $Z_1(T) = A_0 (1 - T/T_c)^{1/2}$, where A_0 is the parameter proportional to the charge density wave amplitude with wave vector Q_0 . As the temperature decreases, the wave vector doubles at $T = 265$ K and the volume jumps up by 3.3% for the composition with $X = 0.3$. This jump is related to the electron compressibility $1/\kappa = d\mu/dn$ under the action of the chemical potential (μ) shift. At a substitute concentration of $X = 0.4$, the wave vector variation in the vicinity of $T \sim 270$ K is (10–17)% and the wave vector of

charge ordering is larger than in the composition with $X = 0.3$ by a factor of 3.

The carrier transport mechanism can be established from the frequency and temperature dependences of the conductivity. The power dependence of the conductivity $\sigma(\omega) = C\omega^s$ is indicative of the hopping conductivity mechanism; in particular, it is attributed to electron hoppings over the localized states with phonons involved [29]. The dispersion dependences of the phonon and magnon energies in an antiferromagnet coincide and the electron scattering on magnons and phonons similarly depends on temperature. In the film with $X = 0.3$, the conductivity dispersion is almost absent; i.e., the conductivity has a constant hopping length and the optimal hopping length is frequency-independent. Using the model of a ferron in the insulating matrix, we can write the resistivity in the form [30]:

$$\rho = kT/128\pi e^2 n^2 \omega l^5 \exp(E_a/kT), \quad (1)$$

where n is the ferron concentration, l is the distance between ferrons, ω is the hopping frequency equal to the phonon frequency, and E_a is the activation energy. The experimental results are described well in the framework of this model below 200 K at an activation energy of $E_a = A (\omega_0 - \omega)^3$, where $\omega_0 = 10^6$ Hz and $\tau_0 \sim 1/\omega_0$ is the time of ferron formation. This is indicative of charge transfer in the phase-separated region. The linear $R(\omega, T)$ dependence above 200 K is caused by the electron scattering on spin excitations. In semiconductors, the carrier scattering on acoustic phonons resulting from the electron–phonon interaction is proportional to $R \sim T^{3/2}$ and the scattering on optical phonons is $R \sim T^{1/2}$ [31] at $T > 2/3 \theta$, where θ is the Debye temperature; for manganese selenide, this temperature is $\theta = 230$ K. In ferromagnetic semimetals, the magnetic field and temperature dependences of the resistivity occur via magnetization: $\rho(T)/\rho(0) = (1 - CM^2) \sim T$ [32]. In the double exchange model, the electrical resistance is completely determined by the carrier scattering on the magnetic moment fluctuations. In the $\text{MnSe}_{1-x}\text{Te}_x$ manganese chalcogenide films, the ac electrical resistance is also caused by the carrier scattering on the fluctuations of antiferromagnetic order, the temperature dependence of which is expressed through the magnetic susceptibility dispersion, e.g., in the Debye model $\chi = \chi_0/(1 + (\omega\tau)^2)$. Above 200 K, the temperature dependence of the resistance is described by the power function $R(\omega, T) = BT^n$ with an increase in the exponent from $n = 1.3$ to $n = 2.2$ with increasing frequency. At low frequencies, the carrier scattering on spin fluctuations prevails, while at high-frequencies, the quadratic $R(\tau)$ dependence is related to the scattering on slow charge fluctuations [33]. In this case, the charge (spin) fluctuations can also be accompanied by noticeable changes in the lattice (polaron effects). As long as

these fluctuations stay incoherent, they will contribute to the resistance. The establishment of coherence at low temperatures switches off this scattering mechanism.

Below 200 K the capacitance slightly grows for the composition with $X = 0.4$ and reaches a plateau for the composition with $X = 0.3$. Upon cooling, the ferron radius decreases and the spin polaron subband is reduced. Then, the degeneracy of the e_g (t_{2g}) states is lifted by the Jahn–Teller interaction. If the splitting of the e_g (t_{2g}) states by the crystal field exceeds the width of a subband of electron excitations in the potential well formed by the electrons localized in the ferron, then it will lead to octahedron straining and film length variation at $T \sim 200$ K.

The carrier transport can be implemented by electron hopping over ferrons or by means of ferron diffusion. These are the activation processes, where the electron mobility is determined as $\mu = \mu_0 \exp(-E_a/k_0T)$, where $\mu_0 = ea^2\nu/k_B T$, ν is the hopping frequency equal to the phonon frequency ($\sim 10^{13}$ Hz), and a is the distance between ferrons [33]. The ferron diffusion can occur due to the interaction with the acoustic spin waves. The ferron flux is proportional to the diffusivity $j \sim D \sim \nu\lambda$, where ν is the spin wave velocity and λ is the ferron free length. The velocity of acoustic spin waves is determined by the spin wave zone width and can be assumed to weakly depend on temperature. The free path length is proportional to the spin correlation radius $\lambda \sim \xi = B/(1 - T/T_N)$, since the ferron energy loss at motion is inversely proportional to the number of spins deviated from the antiferromagnetic positions. The diffusivity of ferrons in the antiferromagnetic matrix increases with temperature: $D \sim 1/(1 - T/T_N)$. The functional temperature dependence of the conductivity can be presented in the form

$$\sigma = A/T \exp(-E_a/kT) + B/(1 - T/T_N), \quad (2)$$

where A and B are the fitting parameters. In the composition with $X = 0.4$, function (2) describes well the experimental results at $A = 6 \times 10^{-4}$, $B = 4.5 \times 10^{-8}$, and $E_a = 0.013$ eV. Above 200 K, the diffusion contribution prevails; below this temperature, the hopping electron tunneling is dominant. The analogous conductivity mechanism is implemented at $X = 0.3$ above 180 K and is described by function (2) with $A = 6.6 \times 10^{-4}$, $B = 2.5 \times 10^{-7}$, and $E_a = 0.013$ eV. The ferron diffusion rate in the film with a tellurium concentration of $X = 0.3$ is higher than in the composition with $X = 0.4$ by an order of magnitude.

The carrier transport in films is implemented by electrons in two subbands, e_g and t_{2g} . This is especially pronounced in the composition with $X = 0.3$, where the resistance sharply drops below 180 K. In [23], the ferromagnetic orbital ordering of electrons was found in the dynamic mean field approximation using the two-orbit Hubbard model with the Coulomb interaction $U/W = 4$ and a Hund's exchange parameter of $J/W = 1.05$ [23]. The resistance increases in the vicinity of the orbital ordering at $T_{or} = 164$ K and the magnetoresistance changes its sign from positive to negative at the transition through the orbital ordering temperature [23]. The inverse susceptibility has an inflection point at this temperature and

the sharp decrease in $\chi^{-1}(T)$ is caused by the ferromagnetic contribution of the orbital magnetic moments.

The negative contribution to the magnetoresistance in the phase-separation region is caused by electrons from the e_g subband and related to the electron hopping mechanism. The functional dependence of magnetoresistance is presented as [33]:

$$MR_n = (\rho(H) - \rho(0))/\rho(0) = \exp(-BH/2T) - 1, \quad (3)$$

where B is determined by the combination of the energies of Coulomb interaction of electrons in a ferron, hopping integral, and spin exchange energy in a ferron and H is the external magnetic field. In the magnetic field, the ferron radius increases and the Coulomb interaction weakens, which leads to a decrease in the electrical resistance at the hopping mechanism. The magnetoresistance is implemented by carriers of two types in two subbands with the orbital ordering (MR_n) and charge transfer between ferrons (MR_p) $MR = MR_p + MR_n$. The experimental data on magnetoresistance are described satisfactorily by the same model in a field of $H = 12$ kOe with a parameter $B = 15$ for $X = 0.3$ and $B = 34$ for $X = 0.4$. The orbital ordering temperature and magnetoresistance decrease with increasing subband width $J < W$ in the model with strong electron correlations. In the composition with $X = 0.4$, the orbital ferromagnetic order will contribute to the magnetoresistance, but much weaker than the electron hopping mechanism. The electrical resistance depends linearly on the magnetic field at the hopping mechanism and quadratically at the orbital electron correlations at $BH \ll T$. The field dependence of magnetoresistance (see the inset in figure 9) near the maximum is described by the function

$$R(H)/R(0) = [1 - BH/2T] - AH^2, \quad (4)$$

with the parameter $A = 0.12$.

The thermopower maxima near the Neel temperature are related to the lattice straining caused by the magnetoelastic interaction. At a temperature difference of $\Delta T = 10$ K, the nonuniform lattice strain is induced near the Neel temperature. The compressibility κ is related to the electron density variation at the chemical potential level μ

$$\frac{1}{k} = \frac{d\mu}{dn} = B,$$

$$d\mu = Bdn = Bn \left(\frac{dV}{V} \right) = Bn \left(\frac{dV}{VdT} \right) dT = Bn\beta dT, \quad (5)$$

where B is the bulk elasticity modulus and β is the thermal expansion coefficient. The temperature dependence of the thermopower is determined by the parameter $\alpha \sim \beta(T)$, if the carrier density and bulk elasticity modulus weakly depend on temperature. Equation (5) describes qualitatively the experimental data.

The small thermopower maxima and thermal expansion anomalies in the temperature range of 265–270 K are caused by the charge density wave variation under the electron–phonon interaction. This transition occurs in a narrow temperature interval and is related to the electron compressibility of a film. Near $T_{or} = 164$ K, the thermopower changes its sign from positive to negative, which is indicative of the carrier sign alternation.

5. Conclusions

The magnetic susceptibility maximum in polycrystalline tellurium-substituted manganese selenide films above the Neel temperature was established, which is related to the spin polaron formation. The thermopower maximum near the Neel temperature was observed, which is caused by the magnetoelastic interaction. In the magnetically ordered region, several types of inhomogeneous electronic states and transitions between them were found. Below the Neel temperature, the phase-separated state with magnetic polarons inside the antiferromagnetic matrix was observed, which is described by the charge density wave. Near 200 K, the localization of polarons is accompanied by the structural lattice deformations, magnetic susceptibility growth, impedance anomalies (the inflection point in the temperature dependence for $X = 0.3$ and the maximum for $X = 0.4$), and crossover of conductivity type from hopping to diffusion. As the temperature decreases, the orbital-ordered state with a quasi-gap in the electron density of states on the Fermi surface forms in the film with $X = 0.3$ and below the Fermi surface in the film with $X = 0.4$. The asymmetry of electron density distribution over the orbital states in the vicinity of the Fermi surface leads to a decrease in the resistance upon cooling and to an increase in the magnetic susceptibility by means of the contribution of orbital magnetic moments. The magnetoresistance changes its sign from positive to negative with increasing temperature near the temperature of ferromagnetic orbital ordering. In a magnetic field, the electrical resistance related to carrier hoppings over ferions decreases. The resulting contribution of these two mechanisms above the orbital ordering temperature leads to the maximum change in the electrical resistance in a magnetic field.

Acknowledgments

The reported study was funded by Russian Foundation for Basic Research (RFBR) according to the research project № 18-52-00009 Bel_a; №18-32-00079 mol_a; № 18-42-240001 r_a; the state order № 3.5743.2017/6.7.

ORCID iDs

O B Romanova  <https://orcid.org/0000-0002-7883-3702>

References

- [1] Sun L *et al* 2012 Re-emerging superconductivity at 48 Kelvin in iron chalcogenides *Nature* **483** 67–9
- [2] Guo J, Jin S, Wang G, Wang S, Zhu K, Zhou T, He M and Chen X 2010 Superconductivity in the iron selenide $K_xFe_2Se_2$ ($0 \leq X \leq 1.0$) *Phys. Rev. B* **82** 180520–4
- [3] Sprau P O, Kostin A, Kreisel A, Böhmer A E, Taufour V, Canfield P C, Mukherjee S, Hirschfeld P J, Andersen B M and Séamus Davis J C 2017 Discovery of orbital-selective cooper pairing in FeSe *Science* **357** 75–80
- [4] Mele P 2012 Superconducting properties of iron chalcogenide thin films *Sci. Technol. Adv. Mater.* **13** 054301–23
- [5] Lindsay R 1951 Magnetic susceptibility of manganese selenide *Phys. Rev.* **84** 569–71
- [6] Ingle Kapil E, EfremD'Sa J B C, Das A and Priolkar K R 2013 Structural and magnetic phase transitions in MnTe–MnSe solid solutions *J. Magn. Magn. Mater.* **347** 68–71
- [7] Gonzalez Szwacki N, Przeździecka E, Dynowska E, Bogusławski P and Kossut J 2004 Structural properties of MnTe, ZnTe, ZnMnTe *Acta Phys. Pol. A* **106** 233–8
- [8] Goswami A and Mandale A B 1978 Electrical properties of manganese telluride films *Japan. J. Appl. Phys.* **17** 473–8
- [9] Efrem D'Sa J B C, Bhohe P A, Priolkar K R, Das A, Paranjpe S K, Prabhu R B and Sarode P R 2005 Low-temperature neutron diffraction study of MnTe *J. Magn. Magn. Mater.* **285** 267–71
- [10] Wei S-H and Zunger A 1987 Total-energy and band—structure calculations for the semimagnetic $Cd_{1-x}Mn_xTe$ semiconductor alloy and its binary constituents *Phys. Rev. B* **35** 2340–2365
- [11] Mahalingam T, Thanikaikarasan S, Dhanasekaran V, Kathalingam A, Velumani S and Rhee J-K 2010 Preparation and characterization of MnSe thin films *Mater. Sci. Eng. B* **174** 257–62
- [12] Angadi M A and Thanigaimani V 1993 Electrical conduction in MnTe and MnSe films *Mater. Sci. Eng. B* **21** L1–4
- [13] Angadi M A and Thanigaimani V 1994 Hall effect in MnTe films *Thin Solid Films* **237** 187–92
- [14] Aplesnin S S, Romanova O B and Yanushkevich K I 2015 Magnetoresistance effect in anion-substituted manganese chalcogenides *Phys. Status Solidi b* **252** 1792–8
- [15] Aplesnin S S, Romanova O B, Korolev V V, Sitnikov M N and Yanushkevich K I 2017 Magnetoimpedance and magnetocapacitance of anion-substituted manganese chalcogenides *J. Appl. Phys.* **121** 075701–7
- [16] Aplesnin S S, Ryabinkina L I, Romanova O B, Balaev D A, Demidenko O F, Yanushkevich K I and Miroshnichenko N S 2007 Effect of orbital ordering on the transport and magnetic properties of MnSe and MnTe *Phys. Solid State* **49** 1984–9
- [17] Kriegner D *et al* 2016 Multiple-stable anisotropic magnetoresistance memory in antiferromagnetic MnTe *Nat. Commun.* **7** 11623–30
- [18] Yuan L, Jalil Mansoor B A, Seng G T, Zhou G and Qian Z 2012 Magnetoresistive effect of a topological-insulator waveguide in the presence of a magnetic field *Appl. Phys. Lett.* **101** 262403–4
- [19] Qu D X, Hor Y S, Xiong J, Cava R J and Ong N P 2010 Quantum oscillations and hall anomaly of surface states in the topological insulator Bi_2Te_3 *Science* **329** 821–5
- [20] Hsieh D *et al* 2009 Observation of time-reversal-protected single-Dirac-cone topological-insulator state in Bi_2Te_3 and Sb_2Te_3 *Phys. Rev. Lett.* **103** 146401–4
- [21] Xu Z J *et al* 2013 Anisotropic topological surface states on high-index Bi_2Se_3 films *Adv. Mater.* **25** 1557–62
- [22] He H T, Liu H C, Li B K, Guo X, Xu Z J, Xie M H and Wang J N 2013 Disorder-induced linear magnetoresistance in (221) topological insulator Bi_2Se_3 films *Appl. Phys. Lett.* **103** 031606
- [23] Peters R, Kawakami N and Pruschke T 2011 Orbital order, metal insulator transition, and magnetoresistance-effect in the two-orbital Hubbard model *Phys. Rev. B* **83** 1–125110
- [24] Zhang J, Ji W-J, Xu J, Geng X-Y, Zhou J, Gu Z-B, Yao S-H and Zhang S-T 2017 Giant positive magnetoresistance in half-metallic double-perovskite Sr_2CrWO_6 thin films *Sci. Adv.* **3** e1701473–7
- [25] Szuszkiewicz W, Hennion B, Witkowska B, Łusakowska E and Mycielski A 2005 Neutron scattering study of structural and magnetic properties of hexagonal MnTe *Phys. Status Solidi c* **2** 1141–6

- [26] Aplesnin S S, Romanova O B, Gorev M V, Vasil'ev A D, Demidenko O F, Makovetskii G I and Yanushkevich K I 2012 Synthesis, structure, and magnetic properties of anion-substituted manganese chalcogenides *Phys. Solid State* **54** 1296–301
- [27] Nagaev E L 1993 Ferron mechanism of charge transport in antiferromagnetic semiconductors and its peculiarities at phase separation *Zh. Eksp. Teor. Fiz.* **104** 2483–98
- [28] Hennion M, Moussa F, Biotteau G, Rodriguez-Carvajal J, Pinsard L and Revcolevschi A 1998 Liquidlike spatial distribution of magnetic droplets revealed by neutron scattering in $\text{La}_{1-x}\text{Ca}_x\text{MnO}_3$ *Phys. Rev. Lett.* **81** 1957–60
- [29] Pollak M and Geballe T H 1961 Low-frequency conductivity due to hopping processes in silicon *Phys. Rev.* **122** 1742–53
- [30] Babushkina N A, Belova L M, Khomskii D I, Kugel K I, Gorbenko O Y and Kaul A R 1999 Low-temperature transition to a metallic state in $(\text{La}_{0.5}\text{Pr}_{0.5})_{0.7}\text{Ca}_{0.3}\text{MnO}_3$ films *Phys. Rev. B* **59** 6994–7000
- [31] Blatt J 1968 *Physics of Electronic Conduction in Solids* (New York: McGraw) p 446
- [32] Furukawa N 1995 Temperature dependence of conductivity in $(\text{La}, \text{Sr})\text{MnO}_3$ *J. Phys. Soc. Japan* **64** 3164–7
- [33] Kagan M Y and Kugel' K I 2001 Inhomogeneous charge distributions and phase separation in manganites *UFN* **171** 577–96